Article

High Temperature Superconducting Non-insulation Closed-loop Coils for Electro-dynamic Suspension System

Li Lu [1], Wei Wu [1]*, Xin Yu [2] and Zhijian Jin [1]

[1] School of Electronic Information and Electrical Engineering, Shanghai Jiao Tong University, Minhang District, Shanghai 200240, China; wei.wu@sjtu.edu.cn
[2] Shanghai Superconductor Technology Co., Ltd., Pudong New District, Shanghai 201203, China; xin.yu@shsctec.com
* Correspondence: wei.wu@sjtu.edu.cn

Abstract: Null-flux Electro-dynamic suspension (EDS) system promises to be one of the feasible high-speed maglev systems above 600 km/h. On account of its greater current-carrying capacity, superconducting magnet can provide super-magnetomotive force that is required for null-flux EDS system and cannot be provided by electromagnets and permanent magnets. There is already a relatively mature high-speed maglev technology with low temperature superconducting (LTS) magnets as the core, which works in the liquid helium temperature region ($T \leqslant 4.2$ K). 2G high temperature superconducting (HTS) magnet winded by $REBa_2Cu_3O_{7-\delta}$ (REBCO, RE=rare earth) tapes works above 20 K region and do not need to count on liquid helium which is rare on earth. This paper designed HTS no-insulation closed-loop coils applied for EDS system and energized with persistent current switch. The coils can work at persistent current model and has premier thermal quench self-protection. Besides, a full size double-pancake module was designed and manufactured in this paper, and it was tested in LN2. The double-pancake module's critical current is about 54 A and it is capable of working at persistent current model, whose average decay rate measured in 12 hours is 0.58%/day.

Keywords: Electro-dynamic suspension; HTS magnets; no-insulation; closed-loop coils; persistent current model

1. Introduction

There are three commonly used suspension technologies in high-speed maglev systems: electro-magnetic suspension (EMS), electro-dynamic suspension (EDS), and high temperature superconducting flux pining suspension [1–6]. EDS is generated from the electric repulsive force between the on-board magnets and the ground coils, and its suspension height can reach 50-100 mm. Compared with EMS, the merits of EDS are that it reduces accuracy requirements for guide rails and that the complex control system is no longer a necessity. Null-flux EDS makes a significant reduction in forward resistance and orbital motor stator cost compared with high temperature superconducting flux pining suspension. Whereas, because of null-resistance characteristics and high current density, the superconducting magnets can provide the huge magnetic momentum which is necessary for null-flux EDS and cannot be provided by normal conductivity magnets and permanent magnets.

The Central Japan Railway Company has been developing a high-speed electric maglev with low temperature superconducting (LTS) magnets as its core, operating in the liquid helium temperature region ($T \leqslant 4.2$ K) since 1970s [7]. The superconducting magnets are closed-loop coils, characterized by self-circulation of current inside the coil, thus enabling passive operation while the vehicle is in motion, and this working mode is known as persistent current mode [8,9]. The use of closed-loop coils and operating in passive persistent current mode can overwhelmingly curtail system's heat loss, and is the preferred mode for on-board conditions. In 2015, the Yamanashi Maglev Test Line (YMTL) set a world record of 603 km/h for the manned vehicle equipped with LTS closed-loop coils. In addition, the 2G high temperature superconducting (HTS) magnets wound

Citation: Lu, L.; Wu, W.; Yu, X.; Jin Z. High Temperature Superconducting Non-insulation Closed-loop Coils for Electro-dynamic Suspension System. *Preprints* **2021**, *1*, 0. https://doi.org/

Received:
Accepted:
Published:

Preprints (www.preprints.org) | NOT PEER-REVIEWED | Posted: 12 July 2021 doi:10.20944/preprints202107.0248.v1

with REBCO tapes can operate at temperatures above 20 K. Compared with LTS magnets, the HTS magnets cooling cost is considerably cut, and China do not need to rely on liquid helium, a non-renewable and scarce strategic resource on earth [10–12] . Open-loop superconducting magnets based on conduction cooling have been developed, but 2G HTS closed-loop magnets still have a long way to be practical, mainly owing to the immaturity of superconducting persistent current switch (PCS) technology, joint technology and quench protection. In recent years, the team of Railway Technical Research Institute has attempted to manufacture HTS closed-loop insulated coils, but due to the large daily decay rate of the coil current, there are still difficulties in producing on-board HTS closed-loop magnets for EDS system [13–16].

The background of this paper is the fabrication of a prototype HTS magnet that can be applied to EDS system, loaded on a maglev test line, with the structure schematically shown in Figure 1. The core of the prototype is the non-insulation closed-loop HTS coils module wound with REBCO tapes without any insulation material filling between the turns of the tapes. Compared with insulated coils, non-insulation coils have the advantage that when thermal quench occurs, the loop current of the coils can pass between the turns, thus bypassing the hot point and providing a good "self-protection" [17]. The HTS coils module works in the solid nitrogen environment with an operating temperature of 20-30 K. In the actual working conditions of the maglev, it is in offline operation (i.e. the refrigeration system does not work). In this paper, a full-size double-pancake (DP) module was successfully designed and fabricated, and it was excited by the thermal-control PCS under LN2 environment. After the excitation, the DP module can work in persistent current mode, and the average decay rate is 0.58%/day during 12 hours, and the joint resistance is about 11.1 nΩ, which meets the design requirements and lays a solid foundation for the fabrication of the prototype HTS magnet.

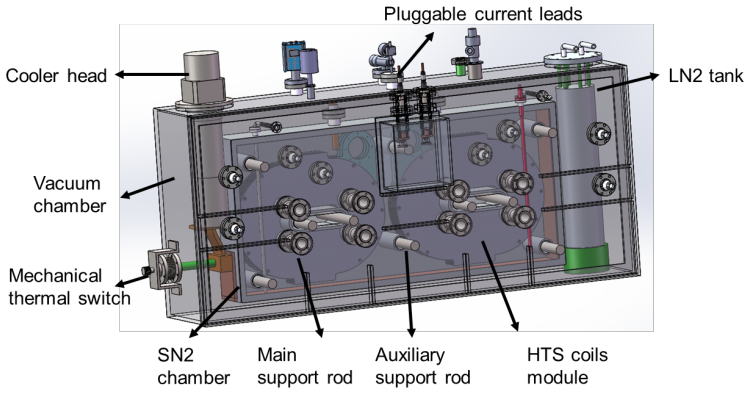

Figure 1. Schematic structure of the HTS magnets prototype.

2. Design of The HTS Coils Module

2.1. Design Requirements and Basic Structure

Based on EDS system's requirements, it is necessary to calculate the basic parameters of the HTS coils module and ground coils, including turns, magnetic momentum, and Geometric dimensions. The levitation and guidance load of EDS system depends on the linear motor stator (figure-eight-shaped coil) surface magnetic field and the total magnetic momentum of the magnets [2,18]. For achieving the levitation and guidance load, the total magnetic momentum of a single pole of an on-board HTS magnet needs to reach 360 kA, and the HTS coils module should be racetrack-shape. Additionally, the axial magnetic flux at the central line 90 mm from the HTS coils module's bottom surface and the axial magnetic flux at the central line of the figure-eight-shaped coil's surface need to exceed 0.7 T and 0.9 T, respectively. Therefore, the length of linear edge and central arc edge is determined as 140 mm and 125 mm, and Figure 2 shows the 2D plot of the HTS coils module. The topology of the HTS prototype coils used for the maglev trial vehicle is

Preprints (www.preprints.org) | NOT PEER-REVIEWED | Posted: 12 July 2021 doi:10.20944/preprints202107.0248.v1

presented in Figure 3, 8 poles in total. Every single pole consists of 3 HTS coils module with 600 turns and works at 200 A, thus the magnetic momentum of a single is 360 kA. Considering the consistence of EDS system, the HTS coils module's decay rate is designed to be below 1%/day in persistent current mode. The Requirements of EDS system and parameters of the prototype coils are shown in Table 1.

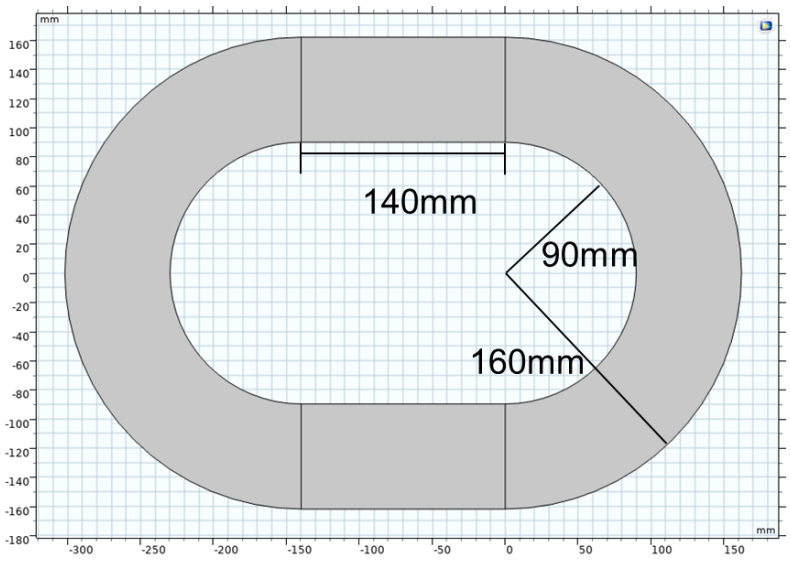

Figure 2. 2D plot of the HTS coils module.

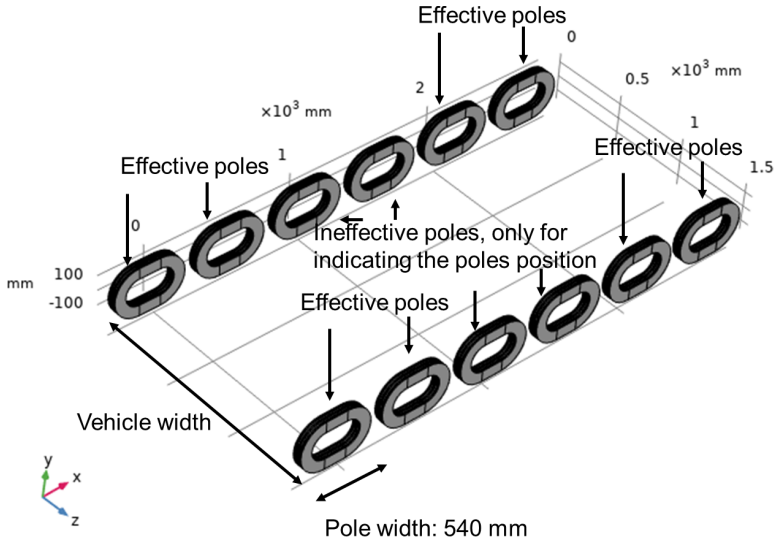

Figure 3. Topology of the HTS prototype coils for maglev trial vehicle (the central four poles don't exist in actual usage, and the topology is just for indicating the poles position relationship).

Preprints (www.preprints.org) | NOT PEER-REVIEWED | Posted: 12 July 2021 doi:10.20944/preprints202107.0248.v1

Table 1. Requirements of EDS system and parameters of the prototype coils.

Parameters	Values
Magnetic momentum of a single pole	$\leqslant$ 360 kA
The axial magnetic flux at the central line 90 mm from the HTS coils module's bottom surface	$\geqslant$0.7 T
The axial magnetic flux at the central line of the figure-eight-shaped coil's surface	$\leqslant$ 0.9 T
Decay rate	$\leqslant$ 1%/day
Poles	8 (4 for each side)
Double pancakes number of a single pole	3
Turns of a double pancake	600
Working current	200 A
Single pole dimensions (Central line)	390·250·66 mm
Spital distance of poles	540 mm

By finite element method (FEM), the electromagnetic properties of the HTS coils module were simulated. Figure 4 and Figure 5 depict the axial magnetic flux distribution on the central line and the surface which are both 90 mm from the HTS coils module's bottom surface, respectively, and the peak value is 0.73 T. Figure 6 and Figure 7 depict the axial magnetic flux distribution on the central line and the surface of the figure-eight-shaped coil, respectively, and the peak value is 0.96 T. The above results cater to the design requirements of the orbital suspension coil and traction system.

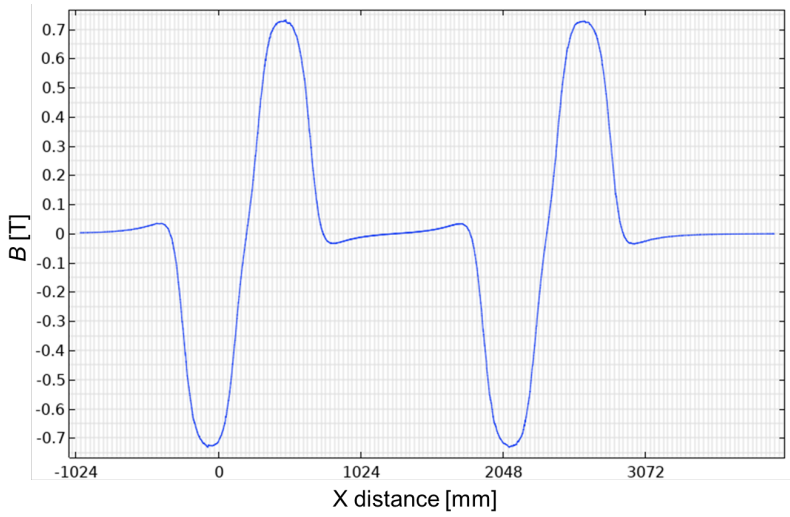

Figure 4. Axial *B* distribution on the central line 90 mm from the superconducting coil module's bottom surface.

Preprints (www.preprints.org) | NOT PEER-REVIEWED | Posted: 12 July 2021 doi:10.20944/preprints202107.0248.v1

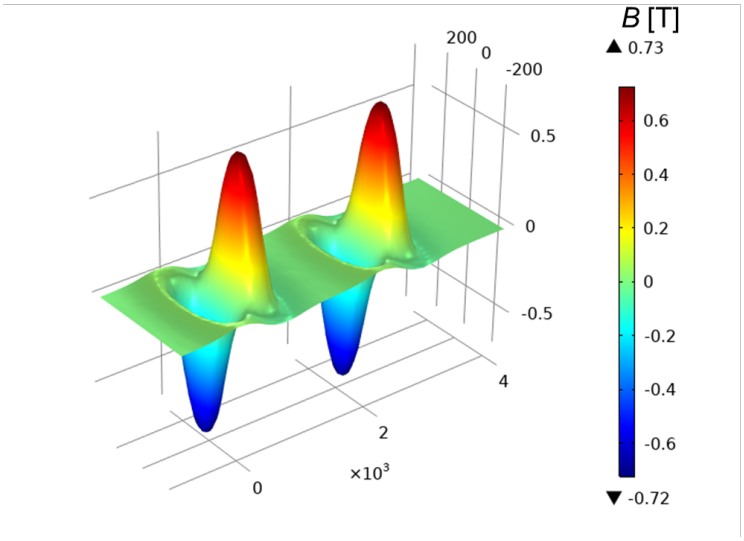

Figure 5. Axial *B* distribution on surface 90 mm from the superconducting coil module's bottom surface.

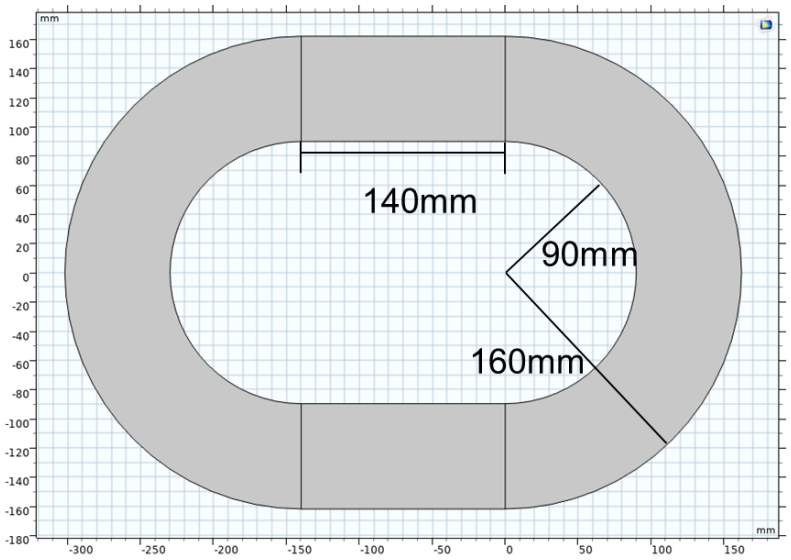

Figure 6. Axial *B* distribution on the central line of the figure-eight-shaped coil's surface.

Preprints (www.preprints.org) | NOT PEER-REVIEWED | Posted: 12 July 2021 doi:10.20944/preprints202107.0248.v1

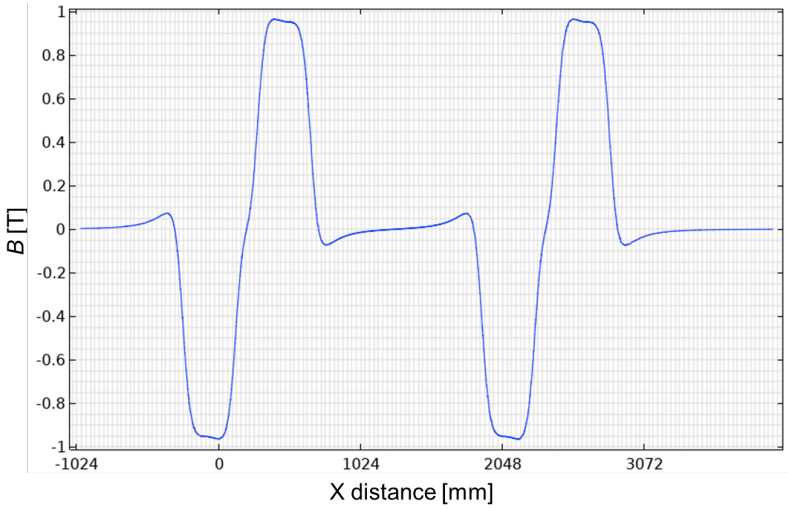

Figure 7. Axial B distribution on the figure-eight-shaped coil's surface.

2.2. Load factor prediction and REBCO tape selection

Considering that the HTS coils module cannot quench in persistent current mode, this paper limits the maximum value of the load factor to below 0.6. The critical current of the 2G HTS tapes has typical anisotropy and is related to the actual operating temperature, known as $I_c - B - theta - T$. The $I_c - B - theta - T$ characteristics of the tape A (Shanghai Superconductor Technology Co., Ltd., TE0133-RRI) is shown in Figure 8, where theta represents the angle between the external magnetic flux and the normal direction of the REBCO tape. Owing to the different manufacturing process, the quality and the $I_c - B - theta - T$ characteristics of the tapes vary from type to type and batch to batch, thus posing difficulties to simulation analysis and actual tape selection. This paper proposes a method for quickly prediction of the $I_c - B - theta - T$ characteristics of different batches of tapes of the same type. For instance, multiplying the $I_c - B - theta$ characteristics curve of tape A at 30 K by a discount factor k (0.73 for example), the $I_c - B - theta$ characteristics curve of Pa1533-A (called tape B) at 30 K and it can achieve relatively low performance. This curve is compared with the actual measured $I_c - B - theta$ characteristics curve of tape-B, as shown in Figure 9, and they are in better agreement.

Preprints (www.preprints.org) | NOT PEER-REVIEWED | Posted: 12 July 2021 doi:10.20944/preprints202107.0248.v1

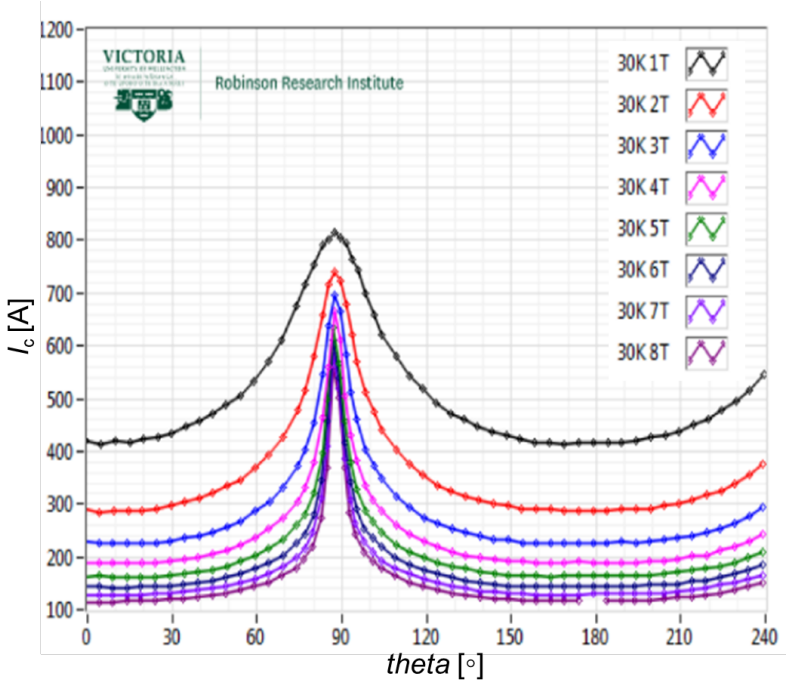

Figure 8. $I_c - B - theta$ characteristics curve of TE0133-RRI tape.

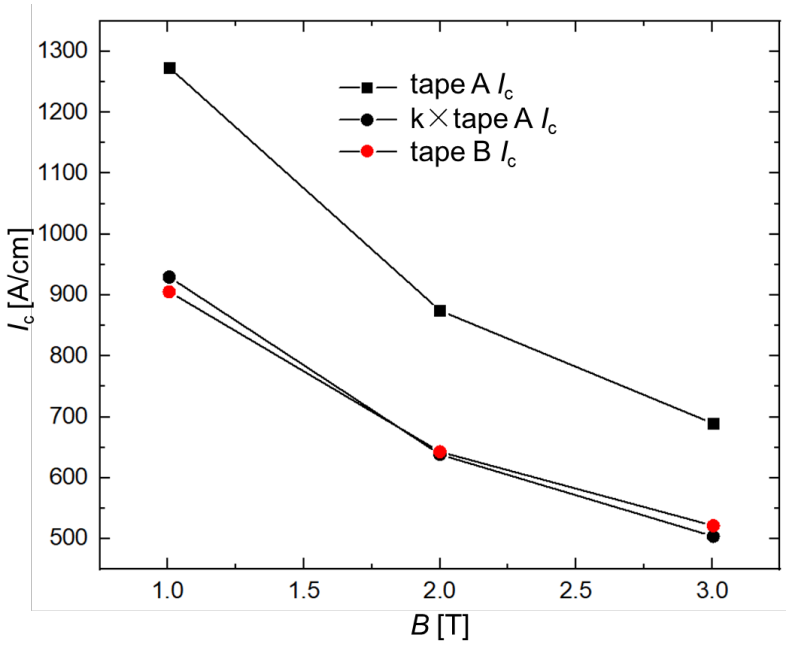

Figure 9. Estimation and verification of different type of HTS tapes' $I_c - B - theta$ characteristics.

The above prediction method can improve the simulation of the distribution of the HTS coils module's load factor and help guide the selection of tapes in practice. For example, the $I_c - B - theta$ characteristics curves of tape A and B are used as input quantities and solved using FEM to obtain the distribution of the load factor of the arc edge of the HTS coils module, as shown in Figure 10**(a)**. Due to the special racetrack-shape of the HTS coils module, the arc edge is the location of the maximum load factor, thus it is used as the load factor indicating area of the HTS coils module. Comparing Figure 10**(a)** and **(d)**, **(b)** and **(e)**, it can be concluded that the closer to the outer side of the single pancake, the larger the load factor; the single pancake wound with higher performance tapes has a smaller

Preprints (www.preprints.org) | NOT PEER-REVIEWED | Posted: 12 July 2021 doi:10.20944/preprints202107.0248.v1

loading factor. Moreover, even if the middle two single pancakes are wound with lower performance tape B, the load factor is still less than 0.5, as shown in Figure 10**(c)**. The above conclusion can guide the actual coil winding using lower performance tapes for the innermost DP and a higher performance tapes for other DPs, thus achieving better economy while ensuring safety of the HTS coils module operation. Limited by the length of tapes, in practice, three separate tapes are connected in series for each single pancake through low resistance joints. Table 2 indicates that the maximum load factor on different location and segment of the single pole wound with tape A and B is less than 0.6, meeting the design requirements.

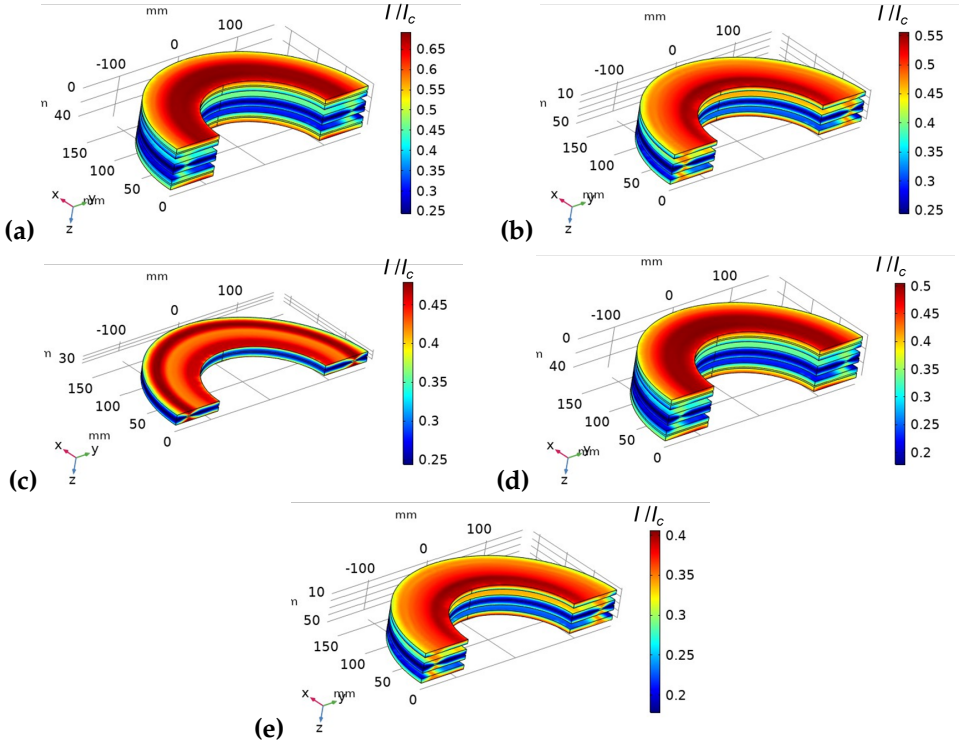

Figure 10. Load factor distribution on arc edge of the single pole at 30 K, for tape B : **(a)** 6 single pancakes; **(b)** Central 4 single pancakes; **(c)** Central 2 single pancakes. For tape A : **(d)** 6 single pancakes; **(e)** Central 4 single pancakes

Table 2. Maximum of load factor distribution on different location and segment of the single pole.

Location and segment	Turns:201-300	Turns:101-200	Turns:1-100
The outside two pancakes (tape A)	0.47	0.51	0.51
The middle two pancakes (tape A)	0.36	0.39	0.41
The central two pancakes (tape B)	0.43	0.45	0.46

3. Fabrication and experiment of DP module

3.1. DP module fabrication

A full-scale non-insulation closed-loop DP module for a HTS prototype magnet was fabricated using a batch of REBCO tapes produced by Shanghai Superconducting Technology Co., Ltd. Figure 11 shows a physical drawing of the DP module with a thermal-control persistent current switch (PCS) on it, which is used for excitation. The DP module is racetrack-shape, and the number of turns of each single pancake is close to 300 turns, and the total inductance is measured about 160 mH. Table 3 lists the parameters of the DP module.

Preprints (www.preprints.org) | NOT PEER-REVIEWED | Posted: 12 July 2021 doi:10.20944/preprints202107.0248.v1

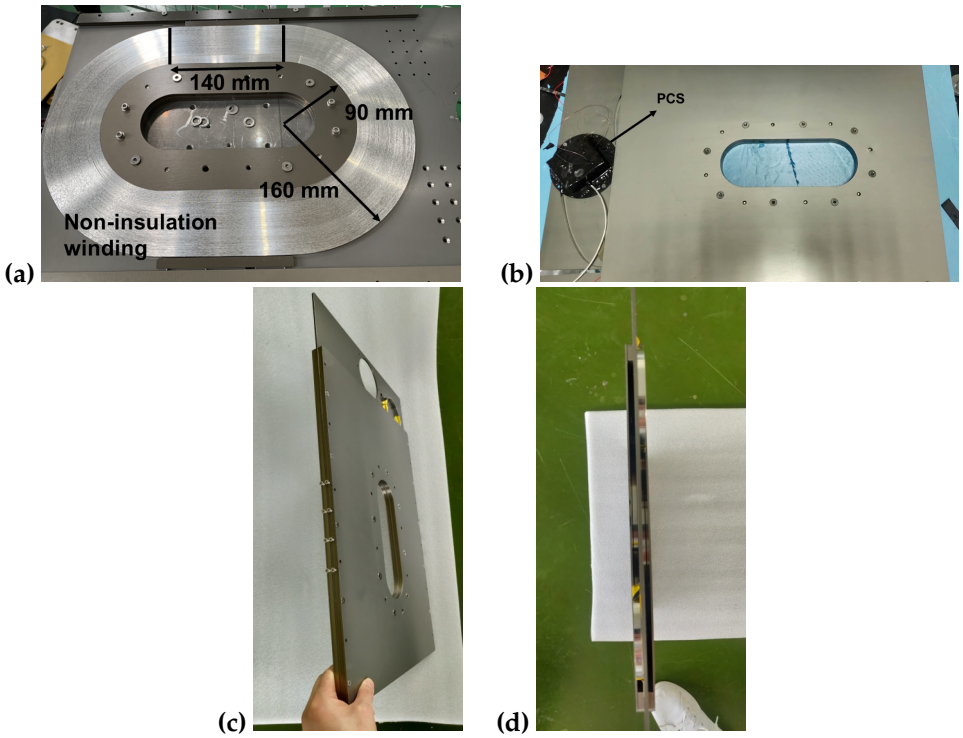

Figure 11. DP Module: **(a)** Non-insulation winding; **(b)** Front view; **(c)** Oblique view; **(d)** Lateral view.

Table 3. Parameters of the DP module.

Parameters	Values
Turns	A: 290, B: 293
Inductance	160 mH
Encapsulation layer thickness	75 μm copper for each side
Tape width/thickness	5.75 mm/0.24 mm
REBCO layer width	4.75 mm
equivalent turn-to-turn resistivity	1.3 $\mu\Omega$·cm^2

The $I_c - B - theta$ characteristics at 77 K for the tape used for winding has been measured experimentally, as shown in Figure 12. By FEM, the characteristics curve is used as the input quantity to simulate the electromagnetic characteristics and the load factor distribution of the DP module (see Figure 13). And Figure 13 demonstrates that the load factor does not outnumber 0.6 when the DP module is operated at a current of 43 A. Whereas, the FEM also calculates the critical current of the DP module about 62 A.

Preprints (www.preprints.org) | NOT PEER-REVIEWED | Posted: 12 July 2021 doi:10.20944/preprints202107.0248.v1

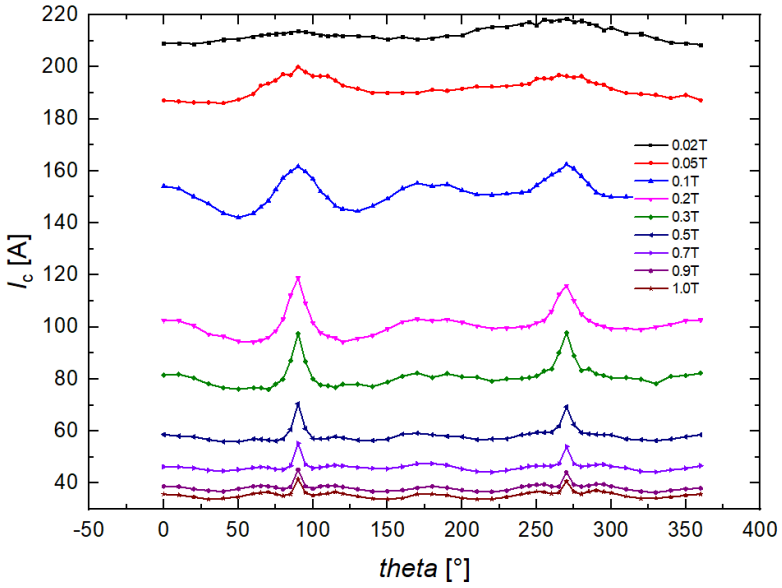

Figure 12. The $I_c - B - theta$ characteristics of tapes winding the DP module at 77 K.

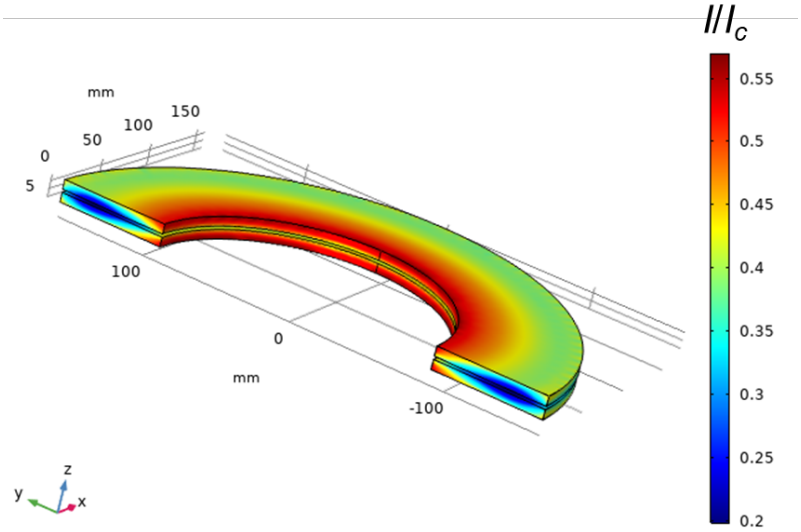

Figure 13. Load factor distribution on arc edge of DP Module at 77 K.

The DP module is discharged under open-loop conditions, and Figure 14 shows the decay curve of the magnetic flux at the center of the DP module under open-loop condition, where B_0 corresponds to the magnetic flux value measured at the end of discharge process. The time constant of the decay of the DP module can be calculated from the curve, and the equivalent turn-to-turn resistance can be calculated based on its total inductance, and finally the equivalent turn-to-turn resistivity is 1.3 $\mu\Omega \cdot cm^2$.

Preprints (www.preprints.org) | NOT PEER-REVIEWED | Posted: 12 July 2021 doi:10.20944/preprints202107.0248.v1

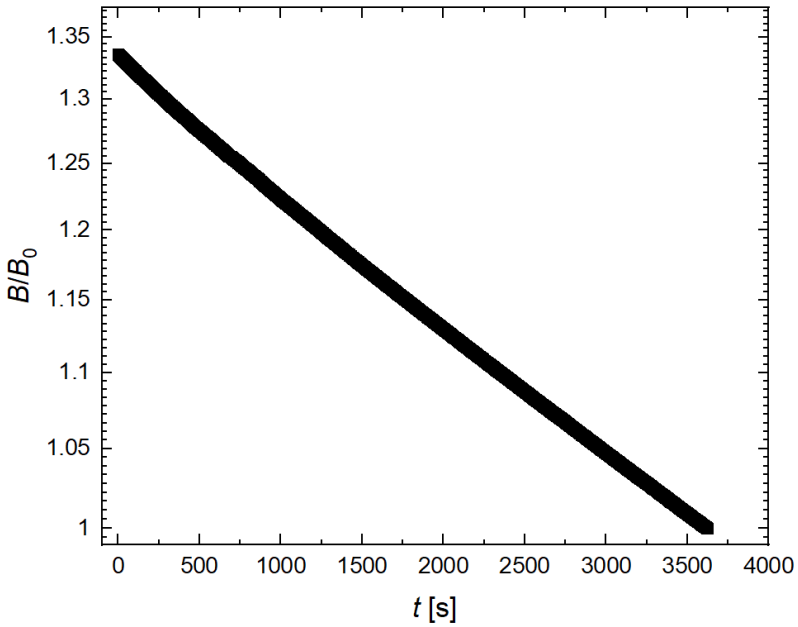

Figure 14. Decay curve of the magnetic flux at the center of the DP module under open-loop condition.

3.2. Experiment of excitation under closed-loop condition

In a bid to quickly test the performance of the DP module, the DP module was tested in LN2 and the thermal-control PCS was used to excite the DP module. The PCS is an essential section of HTS tape with a layer of rigid extruded polystyrene foam (XPS) for thermal insulation wrapped around the outside. By heating the heating film inside the XPS insulation, the quenching of PCS process can be controlled [19]. Figure 15 shows the relationship between the PCS resistance of the DP module and the temperature of the measurement probe inside the PCS when different heating currents (0.4-0.9 A) are applied. The higher the temperature inside the PCS, the higher the PCS resistance is, the shorter the DP module relaxation time, the higher excitation rate is.

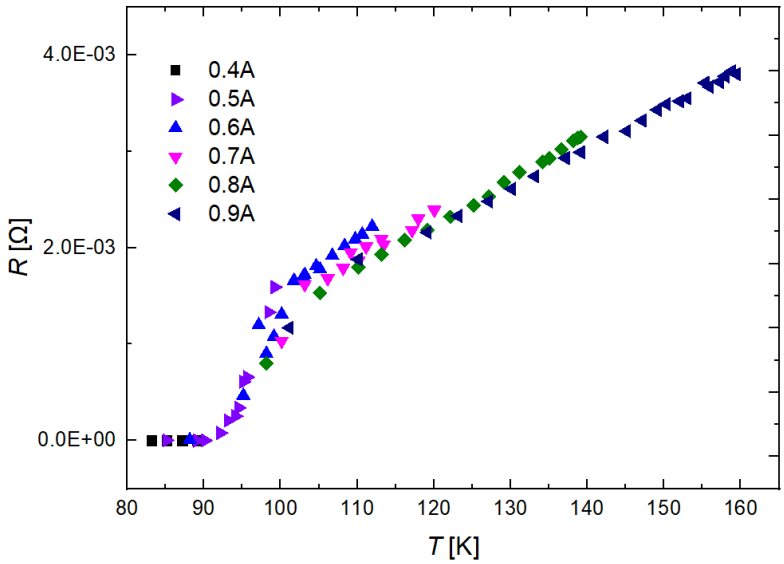

Figure 15. Relationship between the PCS resistance and the temperature of the measurement probe with different current.

Preprints (www.preprints.org) | NOT PEER-REVIEWED | Posted: 12 July 2021 doi:10.20944/preprints202107.0248.v1

Figure 16 shows the variation of the operating temperature of the PCS during the excitation process. The PCS was continuously heated until quenched, and the temperature was kept stable at 1000 s. The current source was excited to the DP module, and the excitation ended at 5000 s after the drop of the temperature of the PCS and the restoration of the superconducting state. The vibration of the output current of the current source and the magnetic flux at the center of the coil during the excitation process are shown in Figure 17. In 2000 s, the current source output current has reached the preset threshold, but the magnetic flux in the center of the coil is still increasing, for which there is a certain inductive resistance of the DP module, which makes the coil turns and the PCS shunt occur, thus the loop current of the coil needs some time to fully be saturated.

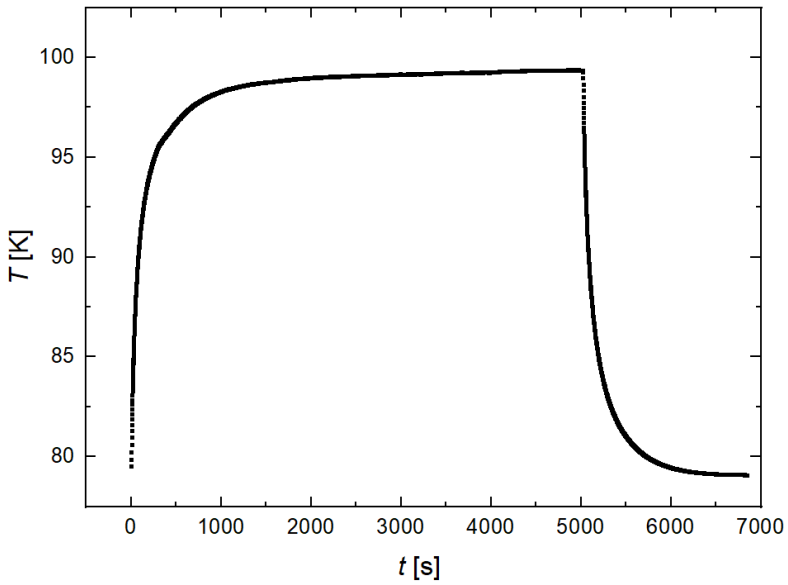

Figure 16. The variation of the operating temperature of the PCS during the excitation process.

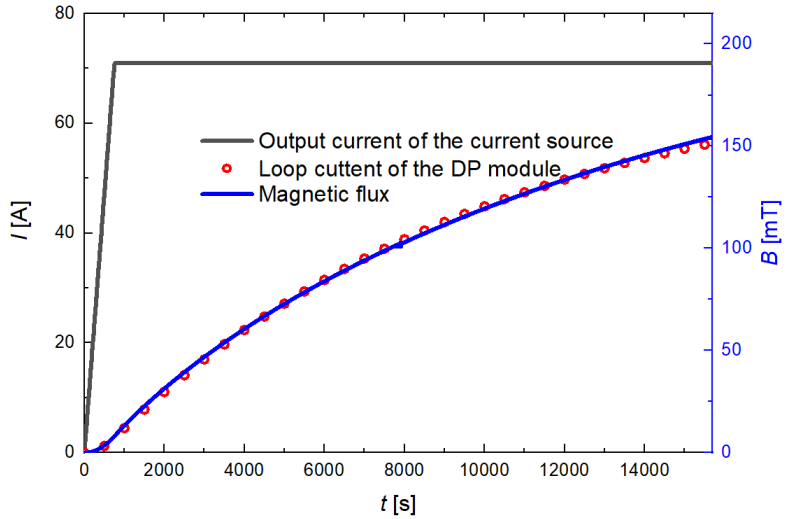

Figure 17. Current source's output current and DP Module's central magnetic flux and loop current.

Regarding the open-loop non-insulation 2G HTS coils, there is a well-established circuit model that is simplified to a series-parallel model of inductance and resistance, so that the charging and discharging characteristics of the coils can be simulated [20]. The PCS branch is added to the set of the circuit model to simulate the excitation process of the closed-loop coil, as shown in Figure 18, where R_{ct} represents the turn-to-turn contact

Preprints (www.preprints.org) | NOT PEER-REVIEWED | Posted: 12 July 2021 doi:10.20944/preprints202107.0248.v1

resistance, L the total coil inductance, and R_{mt} and R_{sc} the matrix resistance and equivalent REBCO layer resistance, respectively. Based on the circuit model, the loop current curve of the DP module can be simulated, as shown in Figure 17. This model also yields values of turn-to-turn resistivity and PCS resistance of 1.8 $\mu\Omega\cdot cm^2$ and 1.0 mΩ, respectively, where the turn-to-turn resistivity is close to the value measured in the open-loop experiment.

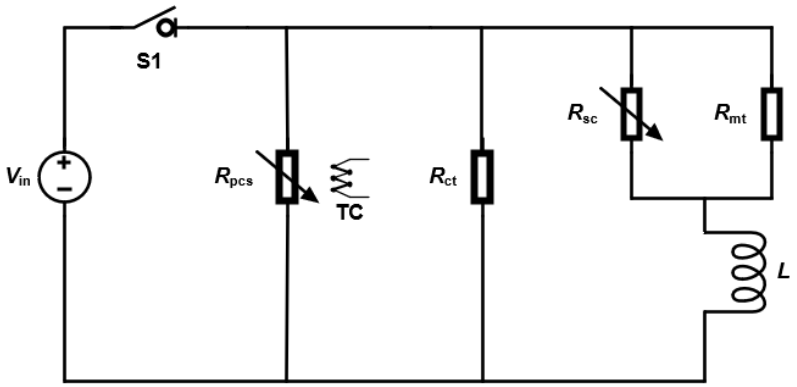

Figure 18. Circuit model of HTS closed-loop coils.

3.3. Persistent current mode

When the excitation is over, it is extremely crucial that the DP module can operate in persistent current mode, which depends mainly on the coil joint resistance. The solder method is adopted to create the low-resistance joints required for closed-loop coils, in which the superconducting surfaces of two tapes are stacked and filled with a relatively low-melting-point solder as the jointing agent, and the REBCO tapes are bonded together by heating and pressurizing them [21]. The V-I curve of a typical joint produced in this paper is shown in Figure 19, and its resistance is 4.6 nΩ measured by the four-lead method.

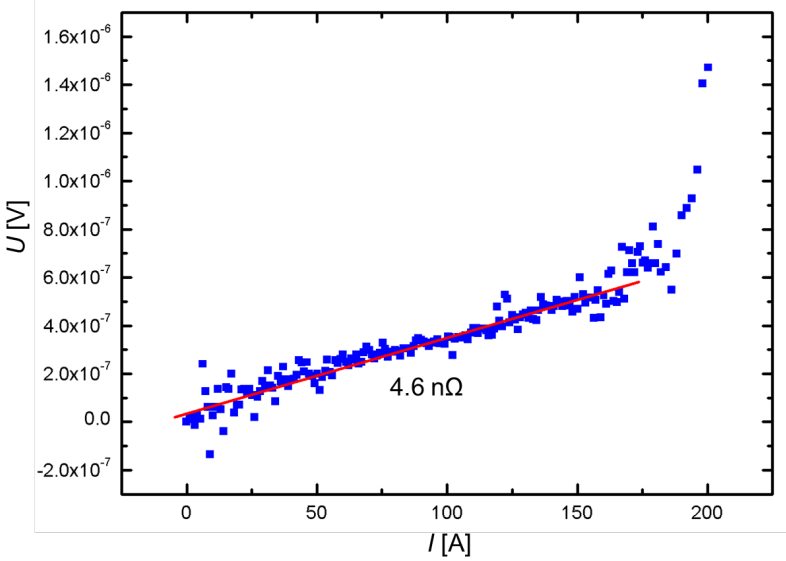

Figure 19. V-I curve of a typical joint.

Figure 20 shows the natural decay curve of the magnetic flux at the measurement probe of the DP module in persistent current mode, and it can be seen that the DP module reached index loss when the magnetic flux outstrips about 148 mT. That is because the internal current of the DP module is close to the critical current, generating a large internal resistance, and the resulting heat loss makes the whole coil lose energy dramatically, and the internal current and the corresponding magnetic flux drops exponentially. The measured

Preprints (www.preprints.org) | NOT PEER-REVIEWED | Posted: 12 July 2021 doi:10.20944/preprints202107.0248.v1

148 mT corresponds to a circulating current of about 54 A in the DP module, indicating that the actual critical current of the coil at 77 K is smaller than the simulation value, mainly because the critical current of the tape is not uniformly distributed and there is a critical current low point. And this is precisely the reason for setting the load factor to no more than 0.6 in the design, leaving a large safety margin.

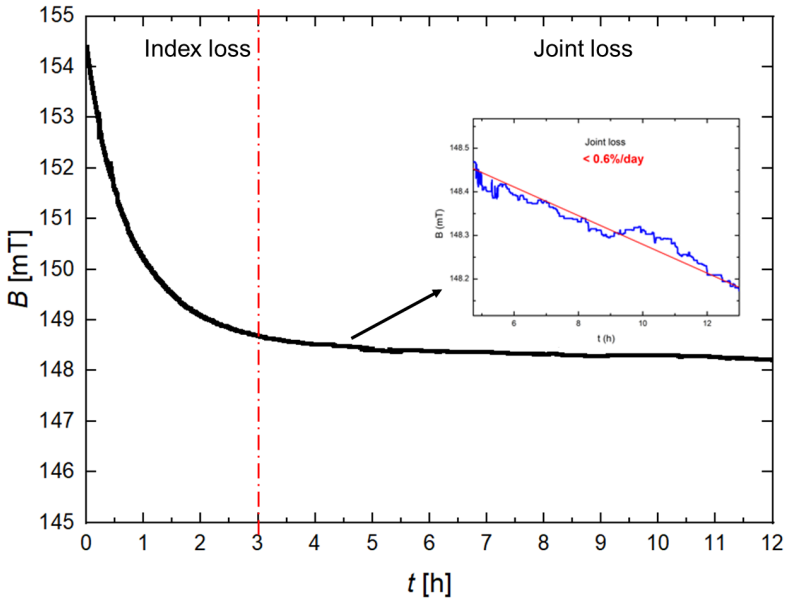

Figure 20. The natural decay curve of the magnetic flux at the measurement probe of the DP module.

When the magnetic flux at the measurement probe is lower than 148 mT, the corresponding internal resistance is small enough, and the decay rate is completely determined by the joint resistance. The experimentally measured average decay rate of the DP module during 12 hours of persistent current mode is about 0.58%/day. The lower daily decay rate is a decisive factor in the commercialization of the closed-loop coil. Based on this decay rate, the joint resistance of the DP module is approximately the same as the typical joint resistance value of the same process measured by the four-lead method.

4. Conclusion

The HTS non-insulation closed-loop coils module was designed and it could be applied to EDS system, which was excited by a thermal-control PCS and could operate in persistent current mode with good self-protection. Whereas, the electromagnetic field and load factor distribution of HTS coils module were simulated and a full-size non-insulation closed-loop DP module was fabricated and tested in LN2 environment to obtain the following main conclusions: 1) Using PCS for excitation, its resistance value determines the coil current relaxation time, and the resistance value of the PCS is about 1.0 mΩ; 2) The experimental critical current of the DP module is about 54 A lower than the simulated value. This is because there is a low critical current point in the used REBCO tapes; hence, a certain margin of load factor needs to be considered in the coil design; 3) After the end of excitation, the DP module could work stably in persistent current mode, and the average decay rate is 0.58%/day measured in 12 hours.

Author Contributions: Conceptualization, L.L. and W.W.; methodology, L.L. and W.W.; software, W.W. and X.Y.; validation, X.Y.; formal analysis, L.L. and X.Y.; investigation, L.L. and X.Y.; resources, W.W> and Z.J.; data curation, X.Y.; writing—original draft preparation, L.L.; writing—review and editing, W.W. and Z.J.; visualization, L.L.; supervision, W.W.; project administration, W.W.; funding acquisition, W.W. and Z.J. All authors have read and agreed to the published version of the manuscript.

Funding: This research was funded by National Natural Science Foundation of China '51977130' and Science and Technology Commission of Shanghai Municipality '17511102300'

Conflicts of Interest: The authors declare no conflict of interest.

References

1. Gong, T.; Ma, G.; Cai, Y.; Qian, H.; Li, J.; Deng, Y.; Zhao, Z. Calculation and Optimization of Propulsion Force of a Real-Scale REBCO Magnet for EDS Train. *IEEE Transactions on Applied Superconductivity* **2019**, *29*. doi:10.1109/tasc.2019.2901564.
2. Bernstein, P.; Noudem, J. Superconducting magnetic levitation: principle, materials, physics and models. *Superconductor Science Technology* **2020**, *33*. doi:10.1088/1361-6668/ab63bd.
3. Ding, J.F.; Yang, X.; Long, Z.Q.; Dang, N. Three-Dimensional Numerical Analysis and Optimization of Electromagnetic Suspension System for 200 km/h Maglev Train Considering Eddy Current Effect. *IEEE Access* **2018**, *6*, 61547–61555. doi:10.1109/access.2018.2876599.
4. Abdelrahman, A.S.; Sayeed, J.; Youssef, M.Z. Hyperloop Transportation System: Analysis, Design, Control, and Implementation. *IEEE TRANSACTIONS ON INDUSTRIAL ELECTRONICS* **2018**, *65*, 7427–7436. doi:10.1109/tie.2017.2777412.
5. Safaei, F.; Suratgar, A.A.; Afshar, A.; Mirsalim, M. Characteristics Optimization of the Maglev Train Hybrid Suspension System Using Genetic Algorithm. *IEEE TRANSACTIONS ON ENERGY CONVERSION* **2015**, *30*, 1163–1170. doi:10.1109/tec.2014.2388155.
6. Long, Z.Q.; He, G.; Xue, S. Study of EDS EMS Hybrid Suspension System With Permanent-Magnet Halbach Array. *IEEE Transactions on Magnetics* **2011**, *47*, 4717–4724. doi:10.1109/tmag.2011.2159237.
7. Nakao, H.; Yamashita, T.; Sanada, Y.; Yamaji, M.; Nakagaki, S.; Shudo, T.; Takahashi, M.; Miura, A.; Terai, M.; Igarashi, M.; Kurihara, T.; Tomioka, K.; Yamaguchi, M. Development of a modified superconducting magnet for Maglev vehicles. *IEEE Transactions on Applied Superconductivity* **1999**, *9*, 1000–1003. doi:10.1109/77.783467.
8. Wang, W.; Lei, Y.; Huang, S.Q.; Wang, P.; Huang, Z.; Zhou, Q. Charging 2G HTS Double Pancake Coils With a Wireless Superconducting DC Power Supply for Persistent Current Operation. *IEEE Transactions on Applied Superconductivity* **2018**, *28*. doi:10.1109/tasc.2018.2793921.
9. Lee, S.; Kim, W.S.; Kim, Y.; Lee, J.Y.; Park, S.H.; Lee, J.K.; Hong, G.W.; Kim, S.; Han, J.; Hwang, Y.J.; Choi, K. Persistent Current Mode Operation of A 2G HTS Coil With A Flux Pump. *IEEE Transactions on Applied Superconductivity* **2016**, *26*. doi:10.1109/tasc.2016.2524519.
10. Kang, L.; Xu, S.; Zhao, Z.W.; Sun, Z.Y.; Zhou, P.B.; Han, L.; Bai, L.Y.; li, J.; Ma, G.T. Experimental Characterization of a No-Insulation HTS Racetrack Coil Subjected to Travelling Magnetic Fields. *IEEE Transactions on Applied Superconductivity* **2020**, *30*. doi:10.1109/tasc.2020.2982395.
11. Li, X.; Li, J.; Zhou, P.B.; Liu, K.; Han, L.; Song, X.L.; Ma, G.T. Decay of Trapped Magnetic Field in Stacks of YBCO Coated Conductors Subjected to Traveling Magnetic Waves. *IEEE Transactions on Applied Superconductivity* **2019**, *29*. doi:10.1109/tasc.2019.2914053.
12. Maeda, H.; Yanagisawa, Y. Recent Developments in High-Temperature Superconducting Magnet Technology (Review). *IEEE Transactions on Applied Superconductivity* **2014**, *24*. doi:10.1109/tasc.2013.2287707.
13. Mizuno, K.; Tanaka, M.; Ogata, M. Evaluation of eddy current heating in a REBCO magnet due to the magnetic field of ground coils for the maglev. *Superconductor Science Technology* **2020**, *33*. doi:10.1088/1361-6668/ab9028.
14. Mizuno, K.; Tanaka, M.; Ogata, M.; Okamura, T. Mechanical Vibration Test of a REBCO Coil Designed for Application to the Maglev. *IEEE Transactions on Applied Superconductivity* **2018**, *28*. doi:10.1109/tasc.2018.2816098.
15. Sugino, M.; Mizuno, K.; Tanaka, M.; Ogata, M. Development of a REBCO HTS magnet for Maglev - repeated bending tests of HTS pancake coils. *Physica C: Superconductivity and its Applications* **2018**, *544*, 13–17. doi:10.1016/j.physc.2017.10.011.
16. Mizuno, K.; Sugino, M.; Tanaka, M.; Ogata, M. Experimental Production of a Real-Scale REBCO Magnet Aimed at Its Application to Maglev. *IEEE Transactions on Applied Superconductivity* **2017**, *27*. doi:10.1109/tasc.2016.2645127.
17. Wang, Y.; Chan, W.K.; Schwartz, J. Self-protection mechanisms in no-insulation (RE) Ba2Cu3Ox high temperature superconductor pancake coils. *Superconductor Science Technology* **2016**, *29*. doi:10.1088/0953-2048/29/4/045007.
18. Hao, L.; Huang, Z.; Dong, F.; Qiu, D.; Shen, B.; Jin, Z. Study on Electrodynamic Suspension System with High-Temperature Superconducting Magnets for a High-Speed Maglev Train. *IEEE Transactions on Applied Superconductivity* **2019**, *29*. doi:10.1109/tasc.2018.2881688.

19. Ling, J.; Voccio, J.P.; Hahn, S.; Kim, Y.; Song, J.; Bascunan, J.; Iwasa, Y. Construction and Persistent-Mode Operation of MgB2 Coils in the Range 10-15 K for a 0.5-T/240-mm Cold Bore MRI Magnet. *IEEE Transactions on Applied Superconductivity* **2015**, *25*. doi: 10.1109/tasc.2014.2370105.
20. Noguchi, S. Electromagnetic, Thermal, and Mechanical Quench Simulation of NI REBCO Pancake Coils for High Magnetic Field Generation. *IEEE Transactions on Applied Superconductivity* **2019**, *29*. doi:10.1109/tasc.2019.2904317.
21. Pan, Y.; Wu, W.; Sheng, J.; Li, X.; Dong, F.; Wang, M.; Zhao, Y.; Zhang, Z.; Li, Z.; Huang, Z.; Hong, Z.; Jin, Z. An equivalent homogenized model for non-superconducting joints made by ReBCO coated conductors. *Superconductor Science Technology* **2018**, *31*. doi:10.1088/1361-6668/aad278.

 doi:10.20944/preprints202107.0248.v1

 doi:10.20944/preprints202107.0248.v1